Appl Phys A (2009) 97: 521–526
DOI 10.1007/s00339-009-5397-6

Applied Physics A
Materials Science & Processing

RAPID COMMUNICATION

Meyer–Neldel rule in fullerene field-effect transistors

Mujeeb Ullah · T.B. Singh · H. Sitter · N.S. Sariciftci

Received: 7 August 2009 / Accepted: 17 August 2009 / Published online: 2 September 2009

Abstract The temperature dependence of the field-effect mobility is investigated in vacuum evaporated C_{60}-based organic field-effect transistors. The results show a thermally activated behavior with an activation energy that depends on the field-induced charge carrier density in the transistor channel. Upon extrapolation of the data in an Arrhenius plot we find an empirical relation, termed the Meyer–Neldel rule, which states that the mobility prefactor increases exponentially with the activation energy. Based on this analysis a characteristic temperature is extracted. The possible implications of this observation in terms of charge transport in fullerene-based field-effect transistors are discussed.

PACS 73.61.Ph · 72.20.Ee · 72.80.Le · 73.20.-r · 71.38.Ht

1 1. Introduction

The charge transport mechanism in organic field-effect transistors (OFET) has been subject of intensive research for some years [1–10]. Although the temperature (T) and gate-voltage (V_G) dependence of the charge carrier mobility (μ_{FE}) of OFETs has been reported [1–7], the charge transport mechanisms in these organic devices are still not fully understood. Observations from thermally activated behavior [2, 3] to T independent transport [4, 5] are reported. It is difficult to obtain an accurate picture of the nature of the transport due to large variations in the experimental data on even nominally the same samples [4, 6]. Studies of contact resistant as a function of applied V_G helped to estimate the most accurate mobility [7, 10–12]. Specific to OFETs, T and V_G dependent μ_{FE} are explained in terms of multiple trapping [3], hopping [8], and Coulomb blockade [9]. A common factor in all these models is the V_G dependence of the activation energy, E_A.

Many organic materials have been reported to follow the Meyer–Neldel rule (MNR), which is a phenomenological model to describe the observed behavior of the material.

The Meyer–Neldel rule for field-effect mobility is described as [13–15]:

$$\mu_{FE} = \mu_o \exp\left(\frac{-E_A}{k_B T}\right) \tag{1}$$

where E_A is the gate-voltage-dependent activation energy, T is the absolute temperature, k_B is the Boltzmann constant. The prefactor μ_o depends exponentially on E_A:

$$\mu_o = \mu_{MN} \exp\left(\frac{E_A}{k_B T_{MN}}\right) \tag{2}$$

Equation (2) which gives the relation between the mobility prefactor μ_o and the activation energy is called the Meyer–Neldel rule. Inserting (2) into (1) gives:

$$\mu_{FE} = \mu_{MN} \exp\left[-E_A\left(\frac{1}{k_B T} - \frac{1}{k_B T_{MN}}\right)\right] \tag{3}$$

As can be seen from (3) at $T = T_{MN}$ all μ_{FE} coincide in one value, namely μ_{MN}, independent of the E_A or V_G. This

M. Ullah · H. Sitter
Institute of Semiconductor and Solid State Physics, Johannes Kepler University Linz, Linz 4040, Austria

T.B. Singh · N.S. Sariciftci
Linz Institute of Organic Solar Cells (LIOS), Institute of Physical Chemistry, Johannes Kepler University Linz, Linz 4040, Austria

Present address:
T.B. Singh (✉)
Molecular and Health Technologies, CSIRO, Bayview Ave., Clayton, VIC 3168, Australia
e-mail: Birendra.singh@csiro.au

characteristic temperature named as Meyer–Neldel temperature and usually reported in terms of the Meyer–Neldel energy as $T_{MN} = E_{MN}/k_B$. The validity of the MNR has been observed in a wide variety of physical, chemical, and biological processes [9]. However, the microscopic origin of the MNR and, therefore, the physical meaning of E_{MN} are still a topic of discussion in literature [13–15].

Among the available charge-transport models for the amorphous materials, multiple trapping and release model (MTR) based on trapping and detrapping of charge carriers with a high concentration of trap states in a narrow energy band can describes the same behavior of the mobility as the MNR assuming an exponential distribution of the density of states. Another theoretical model based on the percolation theory of hopping transport and the field-effect model of transistors was developed by Vissenberg and Matters used to explain the charge carrier transport in amorphous organic materials which usually have a DOS with large number of traps or localized states [8]. Although the MTR model is based on a large number of traps as variable range hopping (VRH), it carries the assumption of a mobility edge with a constant mobility above it and a trap-limited transport of charge carriers in localized states below it and according to the VRH model, the charge carrier transport occurs by hopping of carriers from one site to other site. Another analytical model based on Poole–Frenkel effect gives an inverse variation of the activation energy versus the square root of the electric-field strength [16].

Among the n-type organic semiconductors, fullerenes with a symmetric structure and a low ionization potential (~3.4 eV) show the highest charge carrier mobility 0.6–6 cm^2/Vs [17, 18]. Until now investigations of transport properties of C_{60} were concentrated on diodes [19], OFETs [20–22], and single crystals of C_{60} [23]. Uchino et al. [21, 22] used extended models of VRH and Paloheimo et al. used MNR [19, 20] to describe the charge transport in C_{60} thin films. The drawback of their work is that Uchino et al. were unable to explain the data at T above 100 K and Paloheimo et al. [19, 20] had done the evaluation of E_{MN} by measuring the sheet conductance of the respective devices. However, the extraction of E_{MN} using the sheet conductance is under debate because it may lead to inaccuracy due to a decrease of the effective accumulation channel thickness with increasing V_G [15, 24]. In our previous work [17, 18, 25] we have demonstrated that crystalline quality of C_{60} films could be increased by elevated substrate temperatures during hot wall expitaxy (HWE) growth. Subsequently the field-effect mobility could be increased by factor of ten up to 6 cm^2/Vs.

In this work we report on the systematic investigations on the V_G and T dependence of μ_{FE} in C_{60} based *OFETs*. Field effect mobility, μ_{FE}, is found to be thermally activated with an activation energy strongly dependent on the charge carrier density, N. By extrapolation of the data in the Arrhenius plot according to Meyer–Neldel formalism, the characteristic T_{MN} and E_{MN} were evaluated.

The paper is organized in this fashion: First we describe the evaluation of μ_{FE} in the linear regime as well as in the saturation regime as a function of charge carrier density. Then we evaluated the T dependence of μ_{FE} with the Meyer–Neldel formalism.

2 Experimental procedure

The device scheme of the bottom gate-top contact OFET is shown in the inset of Fig. 1b. Details of device fabrication

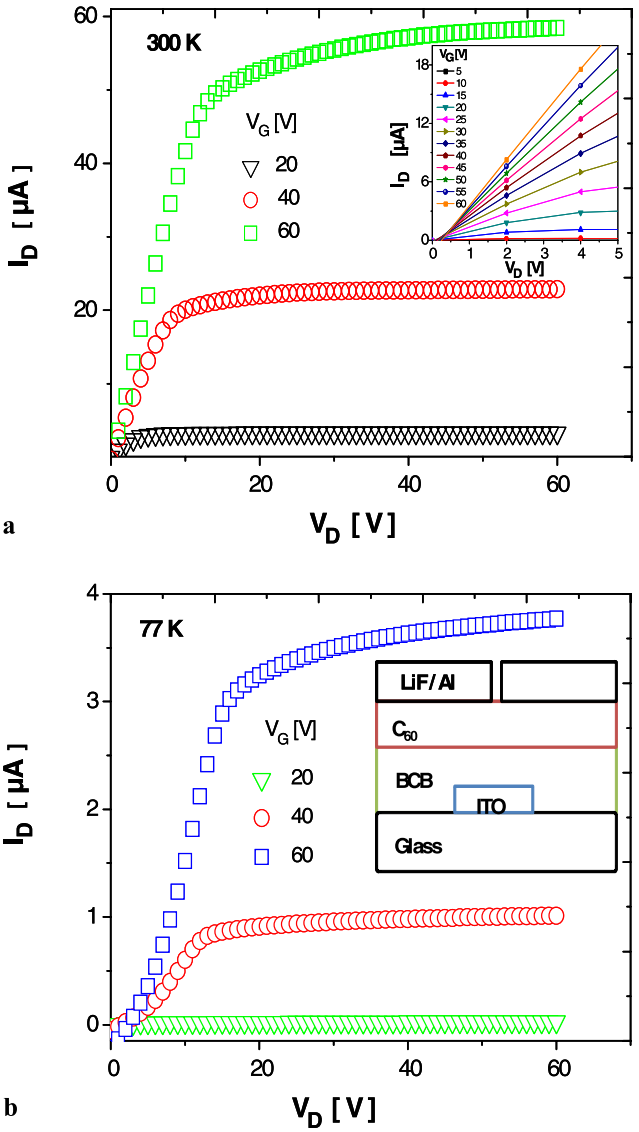

Fig. 1 The output characteristics of the OFET device shown at different fixed V_G (**a**) at 300 K. *Inset* shows linear output curves at 300 K. (**b**) At 77 K showing a sigmoidal curve indicating presence of contact resistance. *Inset* shows the device scheme of the field-effect transistor based on C_{60}

step employed except the deposition of C_{60} are reported previously [17, 18, 25]. In this case the deposition of the C_{60} was done at RT using a Leybold Univex system at a base pressure of 10^{-6} mbar. The resulting C_{60} films were polycrystalline in nature. C_{60} devices which are grown on BCB dielectric without further surface treatment are found to be superior to devices with C_{60} films grown on surface treated SiO_2 dielectric [17, 18]. The reason to choose the top contact geometry in the present experiment is because of low contact resistance of this geometry than the bottom contact geometry as indicated by sigmoidal type I–V characteristics [18]. The completed devices were loaded for electrical characterization in an Oxford cryostat under N atmosphere inside the glove box to avoid exposure to ambient condition. All measurements were carried out at a vacuum of around 10^{-6} mbar and T was changed in a range from 300 to 77 K. The measurements were conducted with a temperature step of 10 K. Between every temperature step there was a time delay of 1 h so that the device got thermally stabilized. The transistor characteristics were recorded by Agilent 2000 SMU.

3 Results

3.1 Evaluation of mobility

Linear regime: The applied gate field in this regime is much larger than the in-plane drift field, which results in an approximately uniform density of charge carriers in the active channel. At low V_D, I_D increases linearly with V_G and is approximately determined from the following equation:

$$I_D|_{V_D \ll V_G} = \frac{W}{L}\mu_{FE} C_i V_D (V_G - V_{th}) \tag{4}$$

where L is the channel length, W is the channel width, C_i is the capacitance per unit area of the insulating layer, V_{th} is the threshold voltage, and μ_{FE} is the field-effect mobility. The latter can be calculated in the linear regime:

$$\mu_{FE,lin} = \frac{L}{W C_i V_D}\frac{\partial I_D}{\partial V_G} \tag{5}$$

Saturated regime: Similarly, μ_{FE} in the saturated regime is given by:

$$I_D|_{V_D \gg V_G} = \frac{W}{2L}\mu_{FE} C_i (V_G - V_{th})^2 \tag{6}$$

Further analyses were done by checking the validity of (6) via local approximation assuming V_G independent of μ_{FE}:

$$\mu_{FE,sat} = \frac{2L}{W C_i}\left(\frac{\delta\sqrt{I_D}}{\delta V_G}\right)^2 \tag{7}$$

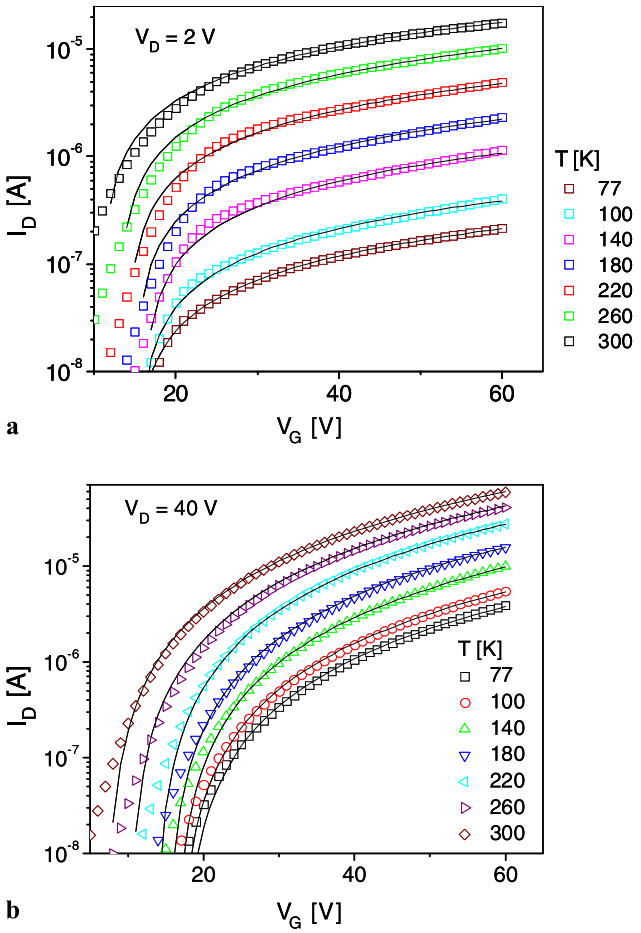

Fig. 2 (**a**) Linear transfer characteristics (*symbols*) of the C_{60} FET with $V_D = 2$ V at various temperatures from 300 to 77 K along with the theoretical fit (*lines*) using (4). The parameters used for theoretical fit are $V_{th} = 11$, 13.5, 14.5, 15.5, 15.5, and 15.5 V; $\mu_{FE} = 0.6$, 0.35, 0.17, 0.082, 0.04, 0.014 cm^2/Vs for $T = 300$, 260, 220, 180, 140, 100 K, respectively; (**b**) The transfer characteristics of device in the saturation regime $V_D = 40$ V at different temperatures (*symbols*) along with the theoretical fit (*lines*) using (6). These devices has $W = 2$ mm; $L = 35$ µm with C_i of 1.2×10^{-9} F/cm^2. The parameters used for theoretical fit are $V_{th} = 8$, 12, 13.5, 15, 15.5, and 16 V; $\mu = 0.61$, 0.5, 0.36, 0.22, 0.14, 0.08 cm^2/Vs for $T = 300$, 260, 220, 180, 140, 100 K respectively

Figures 1a and 1b shows linear and saturated output characteristics of the device at 300 and 77 K at V_G of 20, 40, and 60 V, respectively. The transistor transfer characteristics in both linear and saturation regime at different T is shown in Figs. 2a and 2b, respectively. The experimental data for V_G above the V_{th} are well fitted with the theoretical curves using (4) and (6) for linear and saturated regimes respectively. We further plot experimental μ_{FE} by taking the local slope according to (5) and (7). Such a plot for linear and saturated regimes at various T is shown in Fig. 3a and Fig. 3b, respectively. V_G dependence of μ_{FE} will be considered in more details in the later section. μ_{FE} in both, linear and saturated, regimes is strongly dependent on V_G for $V_G < 16$ V

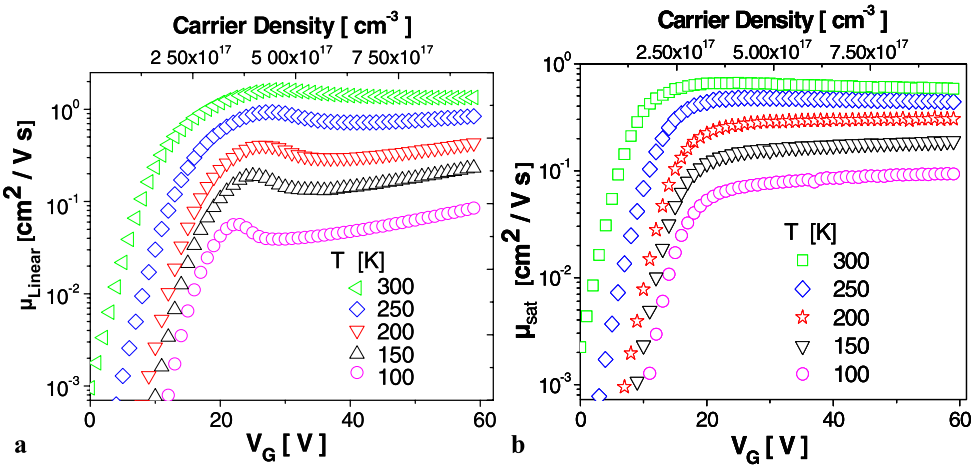

Fig. 3 (**a**) Linear μ_{FE} as a function of carrier density and the V_G at different T by taking the local slopes for the data shown in Fig. 2a. (**b**) Saturated μ_{FE} as a function of carrier density and the V_G at different T for the data shown in Fig. 2b

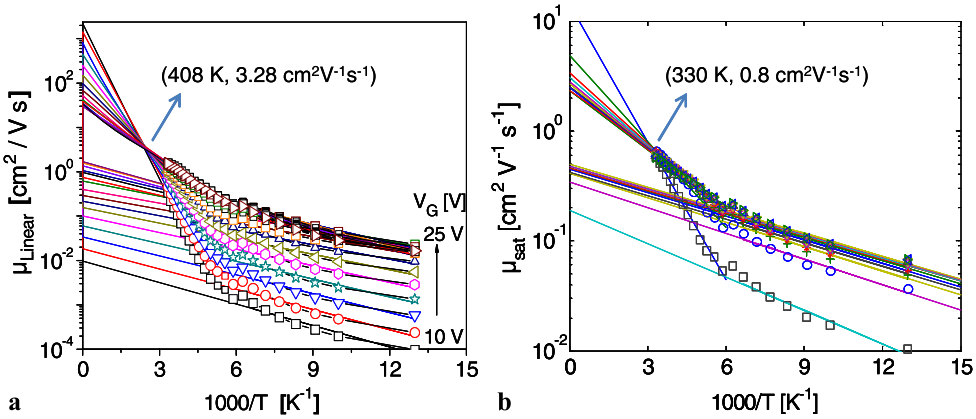

Fig. 4 The Arrhenius plot of μ_{FE} (*symbols*) in (**a**) linear regime at gate voltages of 10 to 25 V with linear fit in the higher T regime. The common point is $(T_{MN}, \mu_{MN}) = (408 \pm 5$ K, 3.25 ± 0.1 cm^2/Vs). The lines drawn at lower T regime is a guide to the eye. (**b**) μ_{FE} in saturation regime at gate voltages of 15, 20, 25, 30, 35, 40, 45, 50, 55, and 60 V. The common crossing point is $(T_{MN}, \mu_{MN}) = (330 \pm 5$ K, 0.8 ± 0.05 cm^2/Vs)

and almost V_G independent μ_{FE} for $V_G > 16$ V. Unlike our previous studies on HWE-grown C_{60} OFETs [25] the present devices show weaker T-dependent μ_{FE} for saturation regime and stronger T-dependent μ_{FE} for the linear regime as shown in the Arrhenius plot of average $\mu_{FE}(T)$ for both regimes in Fig. 4. Details of μ_{FE} (V_G) and μ_{FE} (T) are discussed later.

3.2 Temperature dependence of mobility

In this section we present our data in the framework of MNR which is usually attributed to disorder in the material with an assumption of exponential distribution of trap states. Within the framework of MNR, E_A is strongly dependent on V_G. The Arrhenius plot of the μ_{FE} in linear regime is shown in the Fig. 4a. A linear fit to the data and extrapolating the fit lines we got two set of E_A depending on the range of T. At lower temperatures ($T < 160$ K), the mobility fit lines are almost parallel to each other. It is evident that a clear transition of two E_A occurs at $T \approx 170$ K. The observation of different E_A with different range of T is unclear. It has also been observed previously in 6 T and 8 T semiconductors [26]. At higher T (300–180 K) the fits to the data merges to a one point (T_{MN}, μ_{MN}) which corresponds to ($T_{MN} = 408$ K, $\mu_{MN} = 3.28$) with $E_{MN} = T_{MN}/k_B = 34$ meV. It is to be noted that previous studies have reported similar E_{MN} of 36 meV for C_{60} [19, 20]. Usually the E_{MN} of the organic materials is found in the range of 40 meV [15]. The observation of MNR in OFETs is usually reported in linear regime where the charges are uniformly accumulated (low V_D). Surprisingly we have observed MNR in saturation regime as well (high V_D) as shown in Fig. 4b with a low $E_{MN} = 27$ meV, although there is no well-defined accumulation of charges due to pinch off.

V_G-dependent E_A have drawn a considerable attention in the past due to the fact that it provides the information of nature of charge transport for the given material [12, 25–28]. A plot of E_A versus V_G as shown in Fig. 5a for present devices also shows a strong V_G-dependent E_A. As indicated in Fig. 4a with two distinct slopes give rise to two different E_A over the two T regimes. Between the higher T regime (300–170 K), E_A of 300 meV are reduced to 100 meV upon applying $V_G = 5$–15 V. For the lower T regime (170–77 K) a lower E_A of 40–20 meV is observed. Such an observation of strong V_G and T-dependent E_A can be explained using a model which assumes a semiconductor with Fermi level

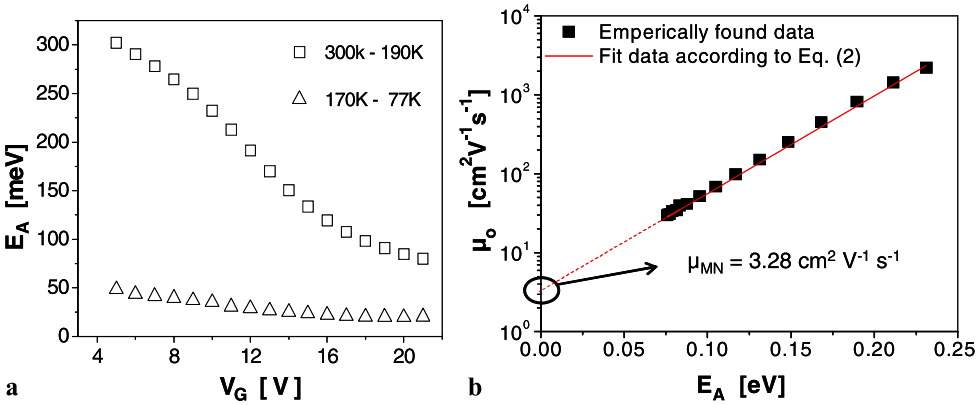

Fig. 5 (**a**) V_G-dependent E_A evaluated using the data from Fig. 4a in two different ranges of T. (**b**) Plot of empirically found μ_o verses E_A (*symbol*) and theoretical fit (*line*) to the data according to (2)

closer to the band edge and upon applying V_G the Fermi level moves through the distribution of band tail states. As a result E_A is reduced as reported in the literature [29]. Similarly other models can be applied to this observation where semiconductor is assumed to have a mobility edge [28]. Charge carriers are assumed to have constant mobility above the mobility edge. Transport of carriers is trap limited with a distribution of localized states that acts as traps. Upon increasing the V_G the Fermi level moves up more and more and trap levels are filled. As a result E_A is reduced as the density of injected charge carriers are increased above the mobility edge [27–30].

Although our studies have shown the V_G-dependent E_A and subsequent models can be applied to explain the observation, the exact picture of DOS is yet to be investigated. As according to the formalism of MNR, from the plot of prefactor μ_o and E_A provides information of whether the semiconductor used is having exponential DOS with large number of trap states [27, 29, 30]. A plot of empirically found prefactor μ_o against the activation energy is shown in Fig. 5b with a theoretical fit line according to (2) which gives a straight line indicating that the MNR holds for the μ_{FE} of C_{60} based *OFETs*. On extrapolating the data we can find the prefactor in (2) μ_{MN} which gives the same and constant value $\mu_{MN} = 3.28\ \mathrm{cm^2\ V^{-1}\ s^{-1}}$ as we can determine it from the common crossing point. The device shows strong activated behavior above 180 K and below this temperature device shows much weaker activated behavior which agrees with results of Paloheimo et al. [20] where the observation of activated behavior is above 250 K and below 200 K, a weakly activated behavior was observed. The V_G dependence of field-effect mobility is explained by several models, i.e., polarons-like states [31], VRH model for exponential distribution of traps [8], extended state conduction with MTR model [32, 33], energy barrier at grain boundary [34], and charge concentration effect at insulator-semiconductor interface [33, 35].

4 Discussion

BCB-based C60 OFETs with LiF/Al contact with W/L ratio of 57 resulted in well-saturated transistor output characteristics as shown in Fig. 1a. As shown in the inset of Fig. 1b, linear characteristics show straight line I–V characteristics at higher V_G which is an indicative of fairly low contact resistant. In contrast to this finding, when C_{60} films which are grown on surface treated SiO_2, I–V characteristics show sigmoidal nature which indicates a larger contact resistance [17, 18]. However, the resistance in BCB-based devices also gets larger at lower temperature as reflected in Fig. 1b by the nonlinear (sigmoidal type) I–V characteristics at low V_D. Transfer characteristics at linear regime as shown in Fig. 2a shows a strong T dependent and large shift of the V_{th} at lower T. Similarly, at saturation regime, a transfer curve with on-off ratio of 10^5–10^6 with saturated on current as high as 0.03 μA/μm at $T = 300$ K. Plot of V_G (or N)-dependent linear μ_{FE} shows a strong V_G and T dependence which can be attributed to defect-induced charge traps in the active semiconducting layer. The basic assumption is that there is a distribution of localized states close to the band edge. At thermal equilibrium, these states are filled up to the Fermi level. As the absolute V_G increase, the Fermi level gradually moves towards the band edge as results more of the empty traps become filled due to charge injection. Accordingly the ratio of free to trap carriers increases, so the effective μ_{FE} increases too. Once the these traps are filled the μ_{FE} reduction at higher V_G is commonly observed which is attributed to the fact that at higher V_G the charge carriers are more close to interface hence more influenced by the interfacial roughness and Coulomb interaction with fixed charges in gate insulator. However, our observation indicates a weak reduction of μ_{FE} once obtained the trap-filled regime.

5 Conclusion

C_{60} OFETs devices are demonstrated to follow Meyer–Neldel formalism with respect to their charge transport prop-

erties for a selective range of temperature. At low temperature charge transport properties could not be explained by MNR. At lower temperatures lower activation arises which leads to almost temperature-independent behavior. As such, a detailed model which explains charge transport in both regimes of temperature will be of further work.

Acknowledgements We acknowledge G.J. Matt, C. Simbruner, Christoph Lackner, and Nifatamah Makaje for stimulating discussion and helps. Financial support for this work was provided by FWF, the Austrian Foundation for Science and Research (NFN projects S9706 and S9711).

References

1. M. Pope, C.E. Swenberg, *Electronic Processes in Organic Crystals* (Oxford University Press, London, 1982)
2. A.R. Brown, C.P. Jarrett, D.M. de Leeuw, M. Matters, Synth. Met. **88**, 37 (1997)
3. G. Horowitz, R. Hajlaoui, P. Delannoy, J. Phys. III France **5**, 355 (1995)
4. S.F. Nelson, Y.-Y. Lin, D.J. Gundlach, T.N. Jackson, Appl. Phys. Lett. **72**, 1854 (1998)
5. I.N. Hulea, S. Fratini, H. Xie, C.L. Mulder, N.N. Jossad, G. Rastelli, S. Ciuchi, A.F. Morpurgo, Nat. Mater. **5**, 982 (2006)
6. L. Torsi, A. Dodabalapur, L.J. Rothberg, A.W.P. Fung, H.E. Katz, Phys. Rev. B **57**, 2271 (1998)
7. R.J. Chesterfield, J.C. McKeen, Ch.R. Newman, C.D. Frisbie, P.C. Ewbank, K.R. Mann, L.L. Miller, J. Appl. Phys. **95**, 6396 (2004)
8. M.C.J.M. Vissenberg, M. Matters, Phys. Rev. B **57**, 12964 (1998)
9. W.A. Schoonveld, J. Wildeman, D. Fichou, P.A. Bobbert, B.J. Van Wees, T.M. Klapwijk, Nature (Lond.) **404**, 977 (2000)
10. P.V. Necliudov, M.S. Shur, D.J. Gundlach, T.N. Jackson, Solid-State Electron. **47**, 259 (2002)
11. K. Seshadri, C.D. Frisbie, Appl. Phys. Lett. **7**, 78 (2001)
12. H. Klauk, G. Schmid, W. Radlik, W. Weber, L. Zhou, C.D. Sheraw, J.A. Nichols, T.N. Jackson, Solid-State Electron. **47**, 297 (2003)
13. W. Meyer, H. Neldel, Z. Tech. **18**, 588 (1937)
14. W.D. Gill, J. Appl. Phys. **43**, 5033 (1972)
15. E.J. Meijer, M. Matters, P.T. Herwig, D.M. de Leeuw, T.M. Klapwijk, Appl. Phys. Lett. **23**, 76 (2000)
16. L. Wang, D. Fine, D. Basu, A. Dodabalapur, J. Appl. Phys. **101**, 054515 (2007)
17. T.B. Singh, N.S. Sariciftci, H. Yang, L. Yang, B. Plochberger, H. Sitter, Appl. Phys. Lett. **90**, 213512 (2007)
18. T.D. Anthopoulos, B. Singh, N. Marjanovic, N.S. Sariciftci, A.M. Ramil, H. Sitter, Appl. Phys. Lett. **89**, 213504 (2006)
19. J.C. Wang, Y.F. Chen, Appl. Phys. Lett. **73**, 948 (1998)
20. J. Paloheimo, H. Isotalo, Synth. Met. **55**, 3185 (1993)
21. K. Horiuchi, S. Uchino, K. Nakada, N. Aoki, M. Shimizu, Y. Ochiai, Physica B **329–333**, 1538 (2003)
22. S. Uchino, S. Hashii, T. Kato, N. Aoki, K. Horiuchi, M. Schimizu, Y. Ochiai, Superlattices Microstruct. **34**, 395 (2003)
23. E. Frankevich, Y. Maruyama, H. Ogata, Chem. Phys. Lett. **214**, 1 (1993)
24. K.L. Ngai, Solid State Ion. **105**, 231 (1998)
25. T.B. Singh, N. Marjanovic, G.J. Matt, S. Günes, N.S. Sariciftci, A. Montaigne Ramil, A. Andreev, H. Sitter, R. Schwödiauer, S. Bauer, Org. Electron. **6**, 105 (2005)
26. G. Horowitz, R. Hajlaoui, R. Bourguiga, M. Hajlaoui, Synth. Met. **101**, 401 (1999)
27. P. Stallinga, H.L. Gomes, Synth. Met. **156**, 1316 (2006)
28. G. Horowitz, R. Hajlaoui, P. Delannoy, J. Phys. III France **5**, 335 (1995)
29. R.J. Chesterfield, J.C. Mackeen, C.R. Newman, C.D. Frisbie, J. Appl. Phys. **11**, 95 (2004)
30. M. Mottaghi, G. Horowitz, Org. Electron. **7**, 528 (2006)
31. H. Bässler, Phys. Status Solidi B **175**, 15 (1993)
32. G. Horowitz, R. Hajlaoui, H. Bouchriha, R. Bourguiga, M. Hajlaoui, Adv. Mater. **12**, 10 (1998)
33. C. Tanase, E.J. Meijer, P.W.M. Blom, D.M. de Leeuw, Org. Electron. **4**, 33 (2003)
34. R. Bourguiga, G. Horowitz, F. Garnier, R. Hajlaoui, S. Jemai, H. Bouchriha, Eur. Phys. J. AP **19**, 117 (2002)
35. P. Stallinga, H.L. Gomes, Org. Electron. **6**, 137 (2005)